Encyclopedia of Interfacial Chemistry: Article

Interaction of ultrafast laser pulses with nanostructure surfaces

A. Lübcke, M. Schnürer, L. Ehrentraut, E. McGlynn, D. Byrne, S. Lowry, R. Wehner, R. Grunwald

Andrea Lübcke
Max Born Institute for Nonlinear Optics and Short-Pulse Spectroscopy,
Max-Born-Str. 2a, 12489 Berlin, Germany
Andrea.Luebcke@mbi-berlin.de

Matthias Schnürer
Max Born Institute for Nonlinear Optics and Short-Pulse Spectroscopy,
Max-Born-Str. 2a, 12489 Berlin, Germany
schnuerer@mbi-berlin.de

Lutz Ehrentraut
Max Born Institute for Nonlinear Optics and Short-Pulse Spectroscopy,
Max-Born-Str. 2a, 12489 Berlin, Germany
ehrentra@mbi-berlin.de

Enda McGlynn
School of Physical Sciences, Dublin City University, Collins Avenue, Dublin 9, Ireland
enda.mcglynn@dcu.ie

Daragh Byrne
School of Physical Sciences, Dublin City University, Collins Avenue, Dublin 9, Ireland
daragh.byrne@dcu.ie

Susan Lowry
School of Physical Sciences, Dublin City University, Collins Avenue, Dublin 9, Ireland
susan.lowry4@mail.dcu.ie

Robin Wehner
Max Born Institute for Nonlinear Optics and Short-Pulse Spectroscopy,
Max-Born-Str. 2a, 12489 Berlin, Germany
robin.wehner@mbi-berlin.de

Ruediger Grunwald
Max Born Institute for Nonlinear Optics and Short-Pulse Spectroscopy,
Max-Born-Str. 2a, 12489 Berlin, Germany
grunwald@mbi-berlin.de

Abstract
The interaction of ultrafast laser pulses with surfaces on the nanoscale paves the way for various innovative technologies in spectroscopy, photovoltaics, photocatalysis, or medicine, to mention only a few. The basic mechanisms, however, are still the subject of intense research. We take a closer look at this topic from different viewpoints. The first aspect is the enhancement of the efficiency of physical or chemical processes by producing local field maxima and resonances at top-down or bottom-up structured surfaces. A further aspect is the dynamic change of optical properties by inducing free carriers and plasmons. Last but not least, permanent nanostructures can be obtained as a result of nano-feedback and self-organization. In high-energy laser physics, all three aspects play a role at once. Therefore, particular attention will be paid to this emerging field.

Keywords
Field enhancement, laser-induced periodic surface structures, nano-feedback, nanorods, nanostructures, nonlinear excitation, particle physics, photocatalysis, proton generation, surface plasmon polaritons, sub-wavelength gratings, surface enhanced Raman spectroscopy, transient changes of optical constants.

Glossary

Anti-Stokes-shift: see → Raman spectroscopy.

Casimir force: Force between bodies in vacuum caused by fluctuating electromagnetic quantum vacuum modes. The Casimir force can be reduced by surface nanostructuring [15].

Double plasma mirror: A plasma mirror is a tool to control the temporal contrast of a laser pulse, i.e. the intensity ratio between ASE (amplified spontaneous emission) or prepulse level and main laser pulse [142]. It basically consists of a glass substrate with an anti-reflection coating. The pulse is loosely focused onto this substrate. At low intensities, before the main pulse, reflection is negligible. However, if the leading edge of the main pulse interacts with the substrate, a plasma is generated. The high density of free electrons strongly increases the reflectivity, i.e. the plasma layer acts like a metal and the main pulse is reflected if the intensity exceeds a critical level. Typically, in laser plasma experiments double plasma mirrors (DPM) with two reflections are applied. A final contrast between main pulse and ASE level > 10^{14} is reached. In our experiments, the DPM reflectivity was about 80%.

Drude theory: The Drude theory [19] describes the transport of free electrons in metals or semiconductors in an external electrical field.

Field enhancement: Local enhancement of the efficiency of physical or chemical processes caused by a higher field density in the proximity of nanostructures or in nanoresonators.

Glancing angle deposition (GLAD): Physical vapour deposition (PVD) technique for the fabrication of nanostructured porous thin films. Roughness and fine structure of the layer can be changed by tuning the deposition angle [143].

Laser-induced periodic surface structures (LIPSS): Surface ripples generated by laser-induced surface plasma waves and ablation [20] and/or thermal re-arrangement of a laser-induced surface instability. The effect was for the first time observed in 1965 by Birnbaum [21]. In detail, the mechanisms depend on laser and material parameters. Two different kinds of LIPSS are usually distinguished with respect to the spatial frequencies: high-frequency LIPSS and low-frequency LIPSS. The responsible formation mechanisms are not identical. Recent experiments indicate combined mechanisms including plasmon excitation, bubble formation and field-induced ablation. Initial random scatterers lead to couple light into surface plasmon polaritons. In a feedback loop, the process repeats self-amplifying. At the positions of maximum field, material is ablated. In the result, ordered grating-like structures are written in the surface. Melting can contribute to a subsequent rearrangement of material.

Laser plasma: Abbreviation for laser produced plasma. A laser plasma is produced during the intense-laser matter interaction. Free electrons are generated via field ionization. For this process to occur, the electric field of the laser pulse must be comparable to the Coulomb field of the nuclei. Depending on the actual field strength, the resulting potential suppresses bound states to different extent. Complete ionization is possible. For the first few hundred fs, these plasmas are far from equilibrium. Once, equilibrium is established, these plasmas are characterized by extremely high electron temperatures, densities and ionization levels.

Metamaterials: Artificial structures with designed values of permittivity ε and permeability μ which are typically not observed in natural materials [144]. Such extended degrees of freedom enable to realize new optical properties, e.g. negative index lenses. The structures are often composed of arrays of nanoelements consisting of metallic and/or dielectric materials.

Nano-feedback: Nano-feedback plays an important role for laser-induced structuring processes as well as for many applications of nanostructures. In the very beginning of the formation of LIPSS, the light is redistributed by of randomly arranged scatterers which act like dipole antennas. Therefore, the feedback is polarization dependent and a preferred orientation of nanoripples is obtained. Sub-wavelength gratings show characteristic spectral resonances and polarization dependencies which can lead to a total absorption of light. The selection, guiding and enhancing of plasmon modes can result from the action of nanostructures as local resonators. A typical effect of nanoresonators is period-splitting. Furthermore, frequency doubling or other nonlinear processes can be locally enhanced close to nanostructures.

Nanorods: Nanorods are rod-like nanoscale solid objects fabricated by chemical synthesis. Such structures have a shape whereby one dimension is significantly greater than the others, typically by a factor of 10 or more, and at least one dimension is of the order of 100 nm or less. Typical materials are semiconductors (e.g. ZnO, TiO_2, Si) or metals (Au). These structures can be fabricated both by top-down lithographic techniques or bottom-up self assembly, or hybrid approaches. The bottom-up self assembly methods are particularly useful and convenient. Controlled self assembly growth can be obtained using chemical bath deposition (CBD) [145] at lower temperatures or vapour phase transport techniques (VPT) [146] or chemical vapour deposition (CVD) at higher temperatures.

Nonlinear nanooptics: Nonlinear optical effects induced or enhanced by nanostructures [147].

Plasma gradient: Abbreviation for plasma density gradient. In the ultra-intense laser solid interaction, a plasma is generated not only at the peak of the laser pulse. Depending on the laser contrast management, even the ASE (amplified spontaneous emission) level can be sufficiently high to ionize the solid to a significant extent already nanoseconds before the main peak interacts with the target. The expansion of this so-called pre-plasma with a specific velocity distribution leads to a spatially dependent plasma density at the plasma-vacuum interface. The exact density profile is of enormous importance for the laser plasma interaction, e.g. for the laser absorption, as well as for ion acceleration.

Photoluminescence (PL): Spontaneous emission from optically excited materials like semiconductors. An enhancement of PL can be achieved by enhancing excitation rates with field-reshaping nanostructures. Increased density of states and enhanced spontaneous emission rate can be obtained by surface plasmons in nanoparticles in composite materials.

Radiation Pressure Acceleration (RPA): Upon reflection of light quanta their momentum is transferred to the "mirror". If the "mirror" is a plasma sheet of low mass and the laser pulse sufficiently energetic, the plasma sheet experiences substantial acceleration and protons can reach very high energies. For a very simple estimate, consider a laser pulse with 1 J energy, a sheet of matter with 10 nm thickness and 3 µm diameter and assume that the laser is completely reflected. With an assumed target density of 1 g/cm³ the light sail model [148] yields a target speed of about 0.15 c, where c is the speed of light. For protons this corresponds to a kinetic energy of 10 MeV. If the laser pulse is applied in less than 100 fs, an enormous acceleration in the order of 10 Exa g (g is the gravitational acceleration on earth, Exa=10^{18}) is acting on the protons.

Raman scattering: see → Raman spectroscopy.

Raman spectroscopy: Raman spectroscopy can probe and measure the frequencies of vibrational or rotational modes of molecules [149]. Therefore, it is a helpful tool in chemistry for the identification of substances. The essential information is a shift in photon energy which depends on the sign of inelastic scattering (Raman scattering) to satisfy energy conservation. If the final vibrational state has a higher or lower energy than the initial state, the shift must be positive (Stokes shift) or negative (anti-Stokes shift), respectively.

Relativistic intensities: A laser pulse is a pulsed electromagnetic field. Those fields act on (free) electrons and accelerate them. If the field strengths are so high that electrons reach relativistic energies, i. e. kinetic energies exceeding the rest energy, within a single cycle, the associated intensities are called relativistic. The scale is set by the relativistically normalized vector potential $a_0 = p_0/(m_0 c)$. Here, p_0 is the maximum (relativistic) electron momentum, c is the speed of light and m_0 is the electron rest mass. In terms of electric field strength E or laser intensity I, a_0 can be rewritten to $e_0 E/(m_0 \omega c) = 0.85 \times 10^{-9} \sqrt{I\lambda^2/(\mathrm{W/cm^2 \mu m^{-1}})}$, where e_0 is the elementary charge, ω is the laser angular frequency and λ is the laser wavelength. For $a_0 << 1$, the electron motion is non-relativistic, while for $a_0 >> 1$, it is strongly relativistic. The case $a_0 = 1$ is reached for laser intensities of $I = 1.4 \times 10^{18}$ W/cm^2 at a laser wavelength of $\lambda = 1$ µm.

Single molecule detection: see → Surface enhanced Raman spectroscopy.

Stokes-shift: see → Raman spectroscopy.

Superhydrophobicity: An enhancement of hydrophobic surface properties can be obtained by roughness or ripples on an optimized spatial frequency scale [150,14].

Surface enhanced Raman spectroscopy (SERS): also referred to as surface-enhanced Raman *scattering*. SERS is a Raman spectroscopy technique with enhanced Raman scattering at adsorbed molecules by local field enhancement at surface nanostructures. Enhancement factors can reach 10^{10} to 10^{14} [1,42,43]. Under optimum conditions, the highly sensitive technique enables to detect *single molecules* [44,45].

Surface plasmon polariton (SPP): SPPs are electromagnetic surface waves that travel along metal-dielectric or metal-air interfaces. This type of wave combines the carrier oscillation in the metal and a charge free electromagnetic wave the air or in a dielectric. At high laser intensities, the required carriers can also be excited in transparent materials via multiphoton absorption. This leads to a transient metallic behaviour which is indicated by a temporal increase of reflection (Drude metals). The spatial periods of SPPs are smaller compared to the periods of the light waves. Therefore, SPPs enable for a stronger localization of electromagnetic field energy compared to free space light waves.

Target Normal Sheath Acceleration: Target Normal Sheath Acceleration (TNSA) is a particular regime of laser driven ion acceleration. Briefly, an ultrahigh intensity laser pulse ($I \sim 10^{19}$-10^{20}W/cm^2) interacts with a target foil of ~1 µm thickness generating hot electrons. This hot electron cloud can penetrate the target foil and escape into the vacuum leaving a charged target behind. At a certain point, the target charge prevents further escaping of even MeV electrons, i.e. those electrons are trapped in the electrostatic field of the target and start to recirculate through the target leading to charge separation on both target sides. The induced electric fields are sufficiently high to ionize atoms at the target surfaces and accelerate ions in the field of the expanding electron cloud. It is important to note that typically accelerated ions stem from a surface contamination layer of hydrocarbons and water molecules. Heavy ions from the target foil are only accelerated if the contamination layer is removed before the experiment or if a different acceleration regime is used (e. g. by inserting ultra-thin target foils of only few tens of nanometers).

XPW front end: Another tool to control the laser contrast [151]. It makes use of crossed-polarized wave generation, a degenerate four-wave mixing process in a nonlinear crystal [152]. The orthogonally polarized wave which is only generated at highest pulse intensities is filtered out by a polarizer. Contrast enhancement by 3-4 orders of magnitude is possible. This results in a final contrast level (after full amplification of the laser pulses) between the main pulse and the ASE level of better than 10^{10}.

1. Introduction

The combination of the unique features of laser light with the specific properties of nanostructured solid materials is a promising field of research with enormous potential for applications in physical and chemical technology, biology and medicine. Nanostructured surfaces enable local reshaping and guiding of light as well as modified optical, mechanical and chemical properties. Therefore, there is an ever increasing spectrum of applications reaching from optoelectronic components with enhanced emission rate or detection sensitivity [1], tailored or broadband absorption [2], high-efficiency solar cells [3] and photocatalysis [4,5] to surface-enhanced spectroscopy techniques, friction control [6], bio-compatibility [7-11] and superhydrophobicity (including anti-corrosion, anti-icing, anti-biofouling, and self-cleaning) [12,13,14]. High-spatial-frequency nanostructures can be tools for quantum experiments [15]. Laser light can be prepared so as to be highly localized in space and time so that nonlinear optical processes can be used to generate far-sub-wavelength structures [16]. The control of polarization [17] and orbital angular momentum [18] of laser beams opens further areas for study and application by adding new free parameters.

One can distinguish between different relevant cases of laser-material interaction. In the first case (a) the material is pre-structured by subtractive or additive techniques (e.g. by drilling nanoholes into a surface or growing nanorods on top). Such nanostructures will be referred to as primary nanostrustures. The interaction of light with nanorods is used for applications like efficiency enhanced frequency conversion, photoelectron emission, sensing or photodynamic therapy. In the second case (b) the optical properties of the material are temporally changed. For example, this is possible by inducing free charge carriers in insulators or semiconductors as described for the stationary case by the Drude theory of metals [19]. Another example is the non-destructive excitation of plasmon-polaritons with sub-wavelength periods at a metal-air interface. Transient nanoperiodic structures will be referred to as transient nanostructures. In the third case (c) the interaction of the laser field with an originally unstructured material leads to the formation of permanent secondary nanostructures. All three cases can be coupled by feedback processes. In one example of which ultimately leads to case (c), the formation of laser-induced periodic surface structures (LIPSS) [20-23], the process starts with a process of the case (b) type and by virtue of a process related to case (a) then ultimately leads to a structure of the case (c) type. At extremely high fields, the transition between the cases can happen nearly instantaneously. In the following paragraphs, the optical properties of nanostructure surfaces and the decisive role of feedback and self-organization for laser-induced nanostructuring will be addressed. A detailed presentation is dedicated to a relatively new field where material sciences, surface chemistry and laser physics meet particle physics. It is shown that dynamic nanostructure formation under the extreme conditions of ultrafast high-field excitation are a promising approach for *secondary sources*, i.e. laser-driven sources of radiation (ions, particles, x-rays etc.) [24-26].

2. Optical properties of nanostructure surfaces

Nanostructured surfaces interact with laser light in a specific way [27]. The degree of randomness of the structures and its control [28] is essential. Scattering, diffraction and absorption depend on wavelength, polarization and (in nonlinear case) on the intensity. For visible or near infrared lasers, surface structures on nanoscale are typically smaller than the wavelength. Therefore, such surfaces

can show effective medium characteristics with structurally modified spectral absorption or reflection. A well-known example are the reduction of reflectance [29,30] or colorizing [31,32] of metals. The observed color effects are related to the excitation of surface plasmon polaritons (SPPs) in surfaces with nanogratings [31]. SPPs are also responsible for coupling effects in arrays of nanogrooves [33]. Blackened materials can serve as a black body radiators in thermodynamics or as absorbers for solar light. Black silicon which exhibits quasiperiodical conical structures is wide-band anti-reflecting and absorbs from visible to near infrared. This makes it interesting for sensing and detection applications. Multifunctional surfaces combine modified optical and tribological properties with each other [34].

For many applications, field enhancement effects or modified optical transfer functions caused by the surface profile [35,36] or local resonant structures [37] enable for significant improvements in sensitivity or efficiency. Laser-induced nanoripples are used to enhance the *extraction efficiency* of light emitting diodes [38]. *Surface enhanced Raman spectroscopy (SERS)* was first reported in 1974 bei Fleischmann [39,40]. Electro-magnetic (plasmonic coupling) and "chemical" (charge transfer) mechanisms are distinguished. Extreme enhancement of Raman lines of 10^6 to 10^{14} is observed [1,41,42]. This enables the detection of single molecules [43-45]. Typical substrates consist of Ag, Au or Cu with nanostructure dimensions in the range of 20-500 nm. In biology, silver citrate or random silver boron aggregates are applied. With Ag necklace structures, enhancement factors of $>10^9$ are realized [46]. A control of nanoscale fields in spectroscopic applications is possible by using nanocrystals [47] or nanoantennas [48]. Surface-enhanced infrared absorption (SEIRA) spectroscopy with tunable nanoantennas was demonstrated [49]. The technical challenge in these cases, however, is still the structuring of sufficiently large areas. Low-cost and one-way substrates can be obtained by replication methods [50]. An alternative method is the formation of laser-induced periodic surface structures (LIPSS) in metals which has been applied to SERS of biomolecules [17]. LIPSS can be replicated and enable for a fast large-area processing. The technique will be described in more detail in the next paragraph.

Nanostructure-supported reaction rate enhancement can also be obtained in *photocatalysis.* Nanostructured porous thin films for catalysis applications can be prepared by glancing angle deposition (GLAD) [18]. Metal oxicde nanotubes and nanorods (nanowires) can be fabricated by

Enhanced photochemical activity was demonstrated with TiO_2 nanotubes [51]. Moreover, TiO_2 nanostructures are interesting for water cleaning and disinfection [52]. Other promising fields of application are water splitting for hydrogen generation [53] or the transformation of atmospheric carbon dioxide into fuel [54,55].

Specific interaction of intense light with nanostructured surfaces (including surfaces decorated with nanoparticles) gives rise to modified spectral response, e.g. for *enhanced ultraviolet photoluminescence* (UV-PL) [56] of large-bandgap materials and *enhanced coherent frequency conversion* like second harmonic generation (SHG) [57-59], third harmonic generation (THG) [60] or high-order harmonics generation (HHG) [61]. Moreover, stimulated emission can be induced in nanomaterials on surfaces [62].

3. Laser-induced periodic surface structures (LIPSS)

The appearance of periodic surface ripples was observed by Birnbaum in 1965 [21]. The mechanisms of LIPSS formation are complex and depend on material type and fine structure [63]. They were explained by the excitation of laser-induced surface plasma waves [20,64-67], Wigner excitons [68],

hydrodynamics [69] and relaxation of laser-induced surface instabilities [70,71]. The interplay of SPPs, hydrodynamic self-organization and material transport processes, all of these models have in common particular feedback loops and self-organization. The plasma wave model starts from statistically distributed scatterers and random matching of the k-vector selection rules by random spatial frequency components convoluted with the dipole characteristics of the scatterers [72,73]. On this basis, the generation of low-spatial-frequency LIPSS (LSFL) can be understood. It is assumed that in the periodical field maxima, photoelectrons are emitted leaving positively charged lattice parts which locally are ablated by Coulomb explosion. By polarization-selective feedback, the angular spectrum narrows and more and more parallel ripples are shaped. Additionally, dynamic polarization flip near plasmon resonance can play a role [74]. The feedback channels are decisive for structural evolution and efficiency [75]. In particular cases, melt-solid patterns with correlated length scales of optical and thermodynamical processes are found [76]. The appearance of high-spatial-frequency LIPSS (HSFL) with far-sub-wavelength features [77-81] is assumed to follow other mechanisms [82]. The formation of LIPSS in transparent large-bandgap materials like ZnO or TiO_2 is possible with ultrashort laser pulses via multiphoton excitation [83,84]. Strong indication was found for the contribution of surface plasmon-polaritons (SPPs) [85-89]. The polarization dependence of LIPSS formation [90] also confirms a plasmonic mechanism. Thermal material modification and rearrangement appear at later time scales but are strongly influenced by plasmons [91]. The ripple orientation, however, can be parallel or perpendicular to the polarization vector so that the scenario seems to be complex in detail (e.g. by a possible influence of SHG [82]). Transient optical parameters by carrier excitation play an important role [60,84,92,93]. LIPSS formation in metals appears to be complex [94]. The excitation of metals requires a relatively strong focusing to couple light into plasmons because of high reflectivity and low initial roughness. Experimental studies with metals like Ti, Al and Au [91,95] indicate that a combination of sub-surface bubble generation and plasmon-related periodical energy insertion results in the generation of isolated or merged nanovoids depending on the fluence. Similar results were obtained for glasses in 3D where bubble formation and rearrangement were found to be related to plasmons as well [96]. The model is also supported by studies of Si dynamics [97].

Double-pulse experiments were performed to explore the mechanisms of LIPSS formation in time domain [98], including polarization sensitivity [99] and two-color excitation [100]. Fig. 1 shows results of a pump-probe diffraction experiment (right side) which was performed to study the dynamics of the ultrashort-pulse LIPSS formation in silicon. The pump laser was an amplified Ti:sapphire laser (central wavelength 800 nm, pulse duration 120 fs). The SHG of a part of the pulses (wavelength 400 nm) was used as probe pulses with variable time delay. The diffraction was detected by a highly sensitive 2D electron multiplying charge-coupled device (EMCCD). The time scales of selected processes are presented in a schematic overview (left side). It is strongly indicated that a combined nonthermal-thermal mechnism has to be assumed with subsequent steps including plasmons in the initial phase and thermal structure formation in stages long after the end of the pulses.

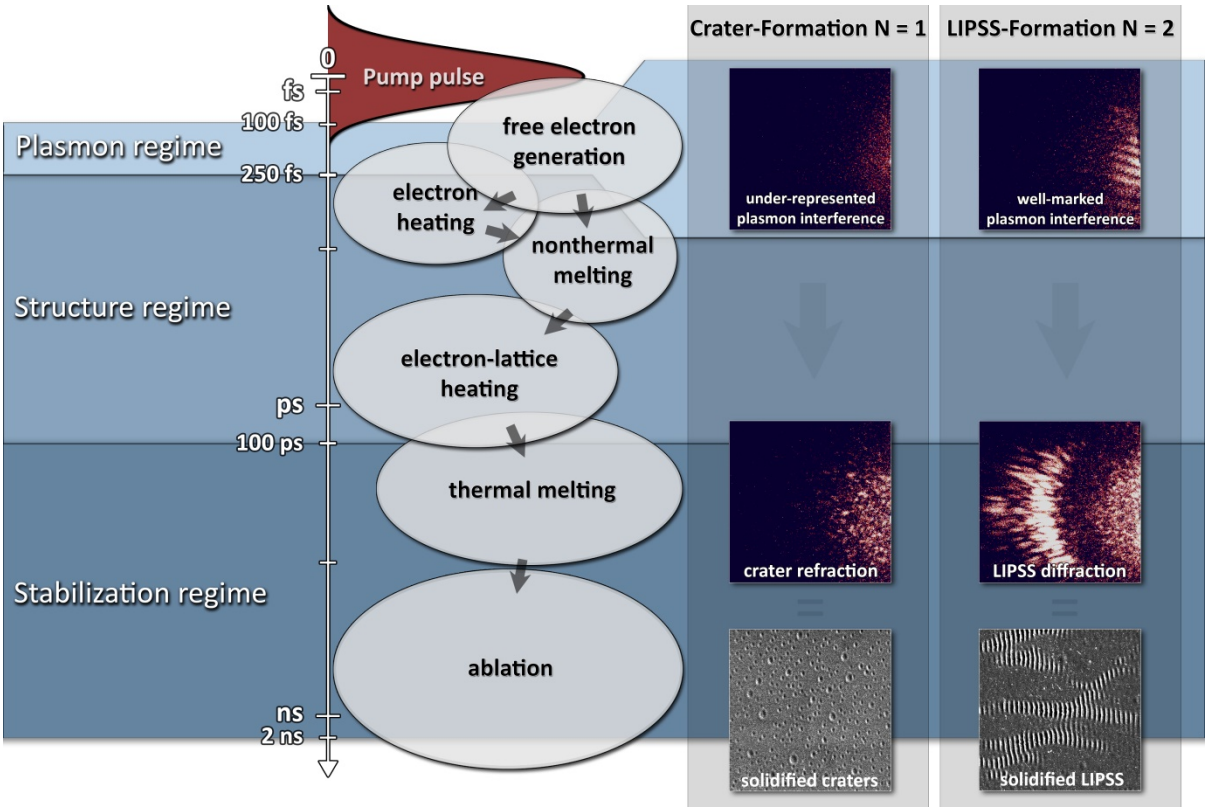

Figure 1 Temporal dynamics of LIPSS formation in silicon. Right side: pump-probe diffraction experiment, left side: corresponding regime and assumed steps of the mechanism (schematically). A combined mechanism is indicated. Plasmons appear during the laser pulse. The nonthermal phase is followed by thermal processes and material re-arrangement.

4. Nanostructured Surfaces in Laser Ion Acceleration

Further promising applications of nanostructured surfaces emerge in laser plasma physics. If ultrahigh intense laser pulses interact with a solid target foil, a hot and dense plasma is generated. These laser produced plasmas give rise to the emission of ultrashort secondary radiation pulses, i. e. Kα radiation [101], bremsstrahlung [102], XUV radiation [103], relativistic electrons [104] and fast ions [105]. The mechanisms leading to those secondary emission are manifold. For ion acceleration for example, target normal sheath acceleration (TNSA), radiation pressure acceleration (RPA) and breakout afterburner (BOA) have been investigated in detail during recent years [106, 105]. Maximum ion energies in such laser plasma accelerators of 93 MeV and above 100 MeV have been demonstrated [107, 108]. What makes this kind of source particularly appealing is its size compared to conventional sources. For example, classical RF accelerators have acceleration gradients of 100 MeV/m. In laser plasmas, 10^4 times larger values are reached. Consequently, much more compact and cost-effective accelerators can be designed. One of the most exciting applications of laser plasma ion acceleration is the hadron cancer therapy [109, 110]. However, this application requires at least two hundred MeV protons and strategies about how to reach such energies with femtosecond lasers targeting the PW-power that are currently built. With plane target strategies, as much as few percent [111, 112] of the laser energy are transferred to protons. The direction of research and development for increasing proton energy and numbers for a given laser energy is

therefore obvious: to improve the conversion efficiency. One possible option is to increase the absorption of laser light, and this is exactly the point where nanostructured surfaces enter the game. Triggered by simulations [113-116], several groups have studied how a nanostructured surface affects laser proton acceleration. Margarone et al. used a 1 µm thick mylar substrate with a single layer of microspheres with diameters of a few hundred nm [117]. With a laser intensity of 5 x 10^{19} W/cm^2 and a laser (p-polarized) incidence angle of 22.5°, they observed an increase of the maximum proton energy from ~5.3 MeV for the plane target to ~8.6 MeV for the 535 nm microspheres. In addition, the total proton beam energy was increased by a factor of 6.3. In a more recent work, Margarone et al. have performed similar experiments but at significantly higher laser intensities of ~7 x 10^{20} W/cm^2 [118]. In this case, they compared a plane 700 nm target with a nanosphere target with an effective thickness of 720 nm where the microspheres had a diameter of 470 nm. At such high laser intensities, an increase of maximum proton energy from about 24 MeV to 30 MeV and an increase of total proton number above 5 MeV by a factor of 4.5 from the plane to the microsphere target, respectively, was observed.

Floquet and co-workers performed similar experiments [119]. An SEM image of one of their samples is shown in Fig. 2a. They used a laser intensity of 2.8 x 10^{19} W/cm^2, different substrate thicknesses (900 nm, 20 µm, 40 µm), microsphere diameters (471 nm and 940 nm) and angles of incidence (10°, 30°, 45°) for both s- and p-polarized laser light.

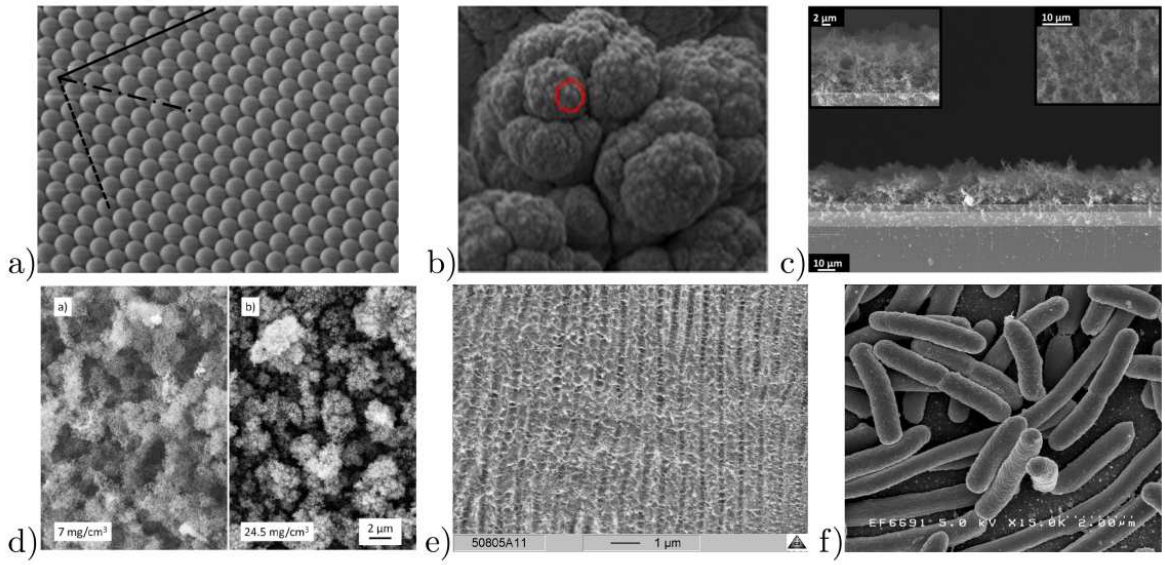

Figure 2 Different nanostructured surfaces used in laser ion acceleration. a) Microsphere targets (with kind permission of J. Appl. Phys. [119]), b) snow target (from [120]), c) foam target (from [121]), d) foam target (from [122]), e) LIPSS (own work), f) E-coli bacteria (Credit: Rocky Mountain Laboratories, NIAID, NIH-NIAID).

The largest effects of the microspheres were observed for the thick substrates and small laser incidence angles. For example, at 10° angle of incidence and for 940 nm microspheres on 20 µm substrate, a relative increase of the proton cutoff energy by at least a factor of 5 was observed for p-polarized laser pulses. In contrast, no beneficial effect of the microspheres was observed for the thin substrate.

Zigler and co-workers applied snow targets (see Fig. 2b) to improve laser proton acceleration [120]. Water vapor was deposited onto a LN2 cooled sapphire substrate. The snow targets possess three different substructure-size scales: pillars of ~ 100 µm, spikes of ~ 10 µm on top of the pillars and whiskers of ~ 1 µm on top of the spikes. With those targets, Zigler et al. enhanced the maximum proton cutoff energy by about one order of magnitude, reaching 20 MeV protons with 5 TW laser pulses.

Yet another approach was chosen by Passoni et al., who used carbon foam targets (cf. Fig. 2c) to improve the energy transfer from the laser to the target [121]. The foams with mass densities of only ~ 7 mg/cm^3 and thicknesses of 12 or 23 µm where grown on 1.5 µm and 10 µm thick aluminum foil, respectively. Passoni et al. have investigated the impact of the foam layer on the maximum proton energy for laser intensities ranging between 5 x 10^{16} and 5 x 10^{19} W/cm^2. They observed a significant increase of proton energy - in particular at low intensities. At 2 x 10^{17} W/cm^2, an increase from 0.3 MeV to 1.2 MeV, i.e. by a factor of 4, is observed. Similar targets were also used by Prencipe et al., who investigated the influence of different foam thicknesses (8, 12, 16, 36 µm) for higher laser intensities of ~ 1 to 4 x 10^{20} W/cm^2 [122]. A SEM picture of their targets is shown in Fig. 2d. The best performance was found for the 8 µm thick foam layer. In this case, the maximum proton energy increased from 22 MeV for the plane 0.75 µm thick Al target to ~ 30 MeV for p-polarized laser irradiation at the highest intensity. A similar result was obtained in terms of maximum C^{6+} energies. Here, an increase from 80 MeV to ~ 120 MeV ~ is observed. The proton numbers increased about 10 times compared to the plane target.

A thin grating target was employed in the work of Ceccotti and coworkers [123]. They could show that also at relativistic intensities a grating can resonantly couple energy into a plasma and cause an enhancement of maximum proton energy. If the laser is incident on the grating target under the resonance angle (+ 30°), maximum proton energies up to 2.5 times larger than in the plane target case were achieved. Under the same angle, a sudden drop of reflectivity is observed. Nevertheless, the maximum proton energies observed from the grating target under resonance conditions did not significantly exceed maximum proton energies from the plane target at larger incidence angle.

All these previously discussed studies concern TNSA. However, it is known that maximum proton energies are actually obtained in the case of RPA. In order to become the dominant mechanism in laser proton acceleration, RPA requires the thinnest possible foils which need to remain close to the transparency limit during the interaction with the ultra-intense laser pulse [124, 111]. In terms of laser parameters, this means that a steep rising edge of the laser pulse, reaching the peak intensity in only a few cycles, is required. These are challenges for laser technologies which have yet to be solved. To overcome those technical issues, Bin et al. have pursued a different approach [125]. They used a near-critical density plasma in which the laser pulse undergoes relativistic self-focusing and pulse front steepening. In order to generate such a near-critical density plasma with suffcient uniformity and lengths of about 1 µm, carbon nanotube foams (CNF) were inserted. This new technology led to significantly enhanced proton and carbon ion energies. For example, 5 µm thick CNF increased proton energies from 10 MeV for a plane target to 15 MeV and C^{6+} energies from 7 MeV/u for a plane target to 20 MeV/u.

Common to all of the previously described approaches is the issue of demanding (and expensive) target preparation processes. Recently, a new approach in target nanostructuring for laser ion acceleration based on LIPSS was investigated by the authors (see above). The specific advantage of our method is that the targets are laser-nanostructured *in situ*. During the first step (nanostructuring), the beam diameter is strongly apertured (from 60 to 6 mm) and the laser energy

on target is further strongly reduced (from 2 J to 10-30 µJ). With these parameters the laser fluence on the sample was adjusted between 2 and 6 J/cm^2. Typically ~20 pulses were applied to generate LIPSS on a 5 µm thick titanium foil with spatial periods of 600 to 800 nm. Typical LIPSS are shown in Fig. 2e). In the second step (ion acceleration), a full-power shot at the complete beam aperture is applied to accelerate protons from the nanostructured target. In between these two steps, no further target alignment or laser manipulation was necessary. In principle, this approach also allows for high repetition rate target solutions. In such a scheme two different lasers (or a TW laser with a kHz frontend) and a tape target system would be employed. One of the lasers (with less pulse energy, but high repetition rate) will generate the nanostructures, while the second one (ultraintense, lower repetition rate) drives the proton acceleration, i.e. between consecutive ultraintense pulses, the sample is (in-situ) nanostructured.

At this point a comment on the applied fluences is needed: in our work, the applied fluence is about twice as high as in other works where LIPSS have been generated [126-131]. However, there is one main difference to those works - and that is that we performed our experiments in vacuum. Our comparative measurements at a kHz laser in air require significantly lower fluences in agreement with previously published work. One possible reason for this apparent discrepancy is that the absence of air deactivates important chemical processes at the plasma surface and thus modifies plasma parameters and the light intensity (due to different nonlinear processes in action).

In our work, we investigated under which conditions the use of nanostructures is beneficial [132]. Besides surface nanostructures there are further options to enhance the coupling between laser and plasma and to optimize the energy transfer from the laser to protons. The most important one is certainly the plasma scale length. We have considered whether nanostructures can further improve the energy transfer if the laser plasma conditions are already optimized by the plasma scale length. If an ultra-intense laser pulse is incident on a solid state target, already the level of amplified spontaneous emission (ASE) or eventual pre-pulses might be sufficiently intense to ionize the target and generate a pre-plasma. This pre-plasma will start to expand generating a plasma density profile that is strongly depending on the full temporal evolution before the peak of the laser pulse. The efficiency of laser absorption strongly depends on the plasma density profile in the vicinity of the critical density, which is the plasma density up to which the laser light can penetrate. On the other hand, for an effcient TNSA acceleration mechanism it is necessary that the target rear surface remains fully intact and a plasma is not formed in this region. From these considerations it becomes clear that there exists an optimal plasma gradient for a given target thickness. Experimental investigations of the interplay between plasma scale length and target thickness were performed by Kaluza et al. and Neely et al. [133, 134].

Performing such experiments at a finite plasma gradient calls in addition for an experimental proof that the nanostructures survive until the peak of the laser pulse interacts with the target. To provide this proof we have investigated the emission of Ti-Kα radiation as function of intensity and for two different plasma gradients, i.e. we performed two sets of experiments: one with the XPW frontend only, and a second one with the DPM in use. Since Kα emission strongly depends on electron numbers and energy distribution function, it is a sensitive measure of laser absorption. For both plasma gradients a significant increase of Kα emission (~ factor 1.5) is observed in presence of the nanostructures even at the highest intensities (8 x 10^{19} W/cm^2). This clearly shows that the nanostructures are functional under both plasma conditions. However, we note that the enhanced absorption may not necessarily be caused by the original structure but possibly by dynamically generated replica resulting from plasma collisions [117].

Our investigations regarding proton acceleration show that nanostructured surfaces can strongly enhance maximum proton energies and numbers, if the laser plasma conditions are not optimal. For example, we have observed an increase of the maximum energy by a factor of ~ 4 and an increase in proton numbers by a factor of 200 at an intensity of 4 x 10^{17} W/cm^2. At optimum conditions on the other hand we did not observe a further increase of maximum energy or proton numbers. This outcome is an important finding. It shows that there are active mechanisms which so far have not been considered in all detail in simulations leading to significant deviations between theoretical predictions and experiment.

Another rather simple method of surface nanostructuring has been used by Dalui et al. [135]. They have applied a coating with e.coli bacteria. E. coli are typically rod-shaped with ~2 µm length and (0.25-1) µm diameter (see Fig. 2f). With this coating and at relatively low laser intensities of only 5 x 10^{17} W/cm^2 they were able to increase maximum carbon ion energies from ~ (30-40) keV (C^+ and C^{2+}; no C^{3+} ions were observed) up to 150 keV (C^+), 400 keV (C^{2+}) and 700 keV (C^{3+}). On the other hand, proton energies could not be increased by the surface coating.

To conclude, all the previously discussed examples of nanostructure applications in laser proton acceleration experiments demonstrate their benefits whenever laser-plasma conditions are not optimal for a plane target. This is the case when the laser intensity or given contrast conditions result in a low absorption due to an overly steep density gradient. Among the different nanostructures tested so far, the LIPSS technique is particularly promising for a high repetition rate target system which is condition precedent for applications that need repetitive particle radiation dose supply.

5. Nanostructure-enhanced XUV emission

Laser produced plasmas are also a source of intense coherent XUV radiation. The emission of high order harmonics is discussed by different models - coherent wake emission (CWE) [136], the relativistically oscillating mirror model (ROM) [103] and coherent synchrotron-like emission (CSE) [137]. The individual models differ in their predictions with respect to emission intensity of different high harmonic orders and emission geometry. These processes are so far investigated only for plane targets. We have started some investigations on HHG from structured targets that promise interesting insights into underlying physics and that we would like to present here.

We studied the XUV emission from so-called nanobrush targets, which consist of ZnO nanorods that are grown on a 30 nm thin Si_3N_4 film. A typical SEM image is shown in Fig. 3. The distance between these nanorods was on the same order of magnitude as their diameter. We used two kinds of nanorods with significantly distinct lengths (100 nm, 400 nm). In addition, we compared the measured XUV spectra from these nanobrush targets to ZnO deposited on Si_3N_4. For the latter samples we estimated a ZnO layer thickness of ~ 50 nm.

The measured XUV spectra are shown in Fig. 4. The emission of high order harmonics is dominant in the range between 50 and 160 nm, while at short wavelength the incoherent plasma emission becomes the dominant contribution to the spectrum. For longer wavelengths, the plasma becomes more and more opaque and the MCP becomes less sensitive which both results in lower XUV photon detection yield. For the nanorod target, we can clearly assign harmonic orders from 5-14, with the maximum intensity in the 8th harmonic. Compared to plane target spectra there are some important differences: First of all, and immediately visible, the intensity of the coherent emission from the sample with longer nanorods is significantly enhanced by more than a factor of 2 with respect to the

best performing flat sample. Furthermore, it seems that there is a shift of spectral intensity: While for the long nanorods the maximum intensity is found in the 8th harmonic, for the other targets (and in particular for the flat ones) the spectral intensity is shifted towards longer wavelengths which reproduces our work on plane targets [139].

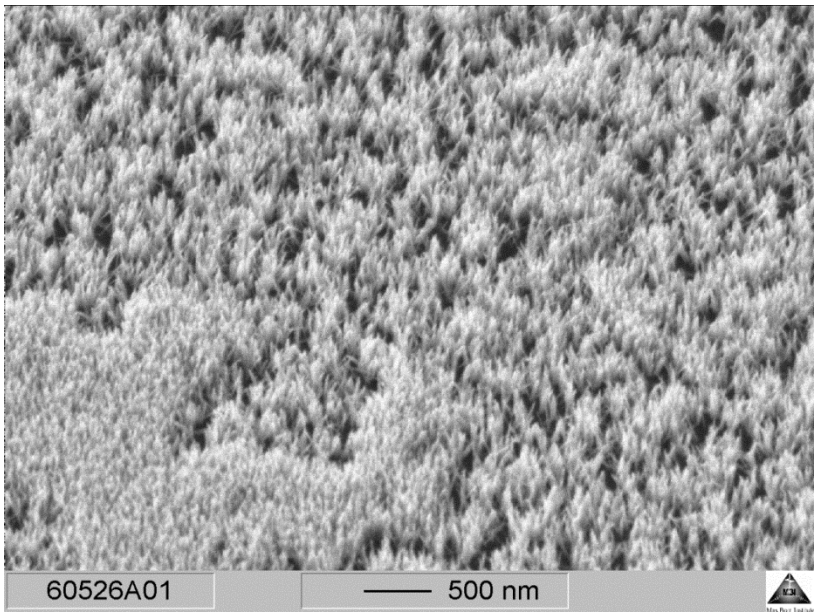

Figure 3 SEM image of a ZnO nanorod sample grown on a 30 nm thick Si_3N_4 substrate.

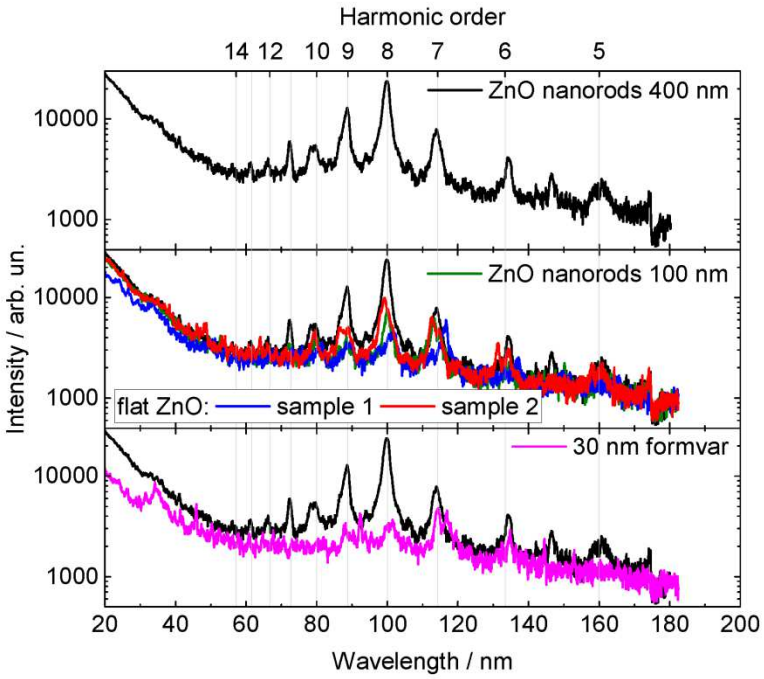

Figure 4 XUV emission spectra for different targets (logarithmic plot). The most efficient long ZnO nanorods (black curve) are compared to short ZnO nanorods (green), flat ZnO layers (red and blue) and formvar (polyvinyl formal resin, pink). All ZnO layers were prepared on a 30 nm thick Si_3N_4 substrate.

Both observations show that ZnO nanorods have an impact on the XUV emission. First results from simulations are available concerning the physical origin of the XUV emission from nanobrush targets [138]. However, that work mainly concentrates on the emission of coherent betatron radiation. The central idea is that the laser field and the electrostatic field of the nanorods drive electrons into coherent betratron oscillations. These simulations assumed significantly larger distances between the nanorods than those available in our targets. Concerning HHG emission from nanostructured targets, we are not aware of any theoretical work in the literature as yet. There are however some works about the HHG emission from planar targets that focus on a CSE-like model [137]. Experiments with flat targets show enhanced high harmonic emission, if target pre-expansion was initiated by a pre-pulse [139]. One way to discuss our results from the nanorod target may therefore be in the context of a reduced effective density. According to the CSE model, such a density modification can enhance the emission. Nevertheless, to what extent we can exclude or have to include a CWE process in case of the nanostructured samples is not clear at the moment. The emission of an 11/2 harmonic is not intuitively in line with the CWE model but may stem from a two-plasmon decay [104]. The shift in spectral density also indicates that the underlying processes and mechanisms may be different. However these studies represent only a starting point and the very first results on this interesting and promising application of nanostructures in laser plasma XUV sources. More experimental and theoretical studies are necessary to unravel the complex plasma dynamics involved and to yield a comprehensive understanding of those processes.

6. Summary and outlook

Nanostructured surfaces enable a variety of applications by enhancing the efficiency of physical, chemical and biomedical processes. In addition to this, nanostructures can be generated by the laser irradiation of materials. In both cases, intense ultrashort pulses open specific nonlinear excitation channels. Under extreme conditions with respect to pulse duration and field intensity, the laser-matter interaction is highly complex. The use of permanent or transient nanostructures promotes the realization of more efficient or compact secondary sources for the characterization and modification of materials. Most of the specific light-nanostructure interactions addressed here are related to electric field effects. It has to be mentioned, however, that there is also a great potential for applications in the case of laser-induced magnetic field phenomena such as plasmon enhanced transient magnetization, which is of importance for high-capacity data storage [140]. Tailored metamaterials [141], bio-mimetic structures and functional surfaces with tunable properties are other intriguing targets for future research.

The authors are grateful for support and resources from Max Born Institute for Nonlinear Optics and Short-Pulse Spectroscopy, for the kind permissions to reproduce figures from the Journal of Applied Physics (AIP Publishing), Physical Review Letters (APS Publishing), Plasma PhysIcs and Controlled Fusion (IOP Publishing) and Rocky Mountain Laboratories, and for financial support by the Deutsche Forschungsgemeinschaft (DFG; reference numbers GR 1782/12-2 and AN 1055/2-1) and LaserLab Europe (reference numbers 284464 and 002096).

References

[1] Blackie, E. J., Le Ru, E. C., and Etchegoin, P. G. (2009). Single-molecule surface-enhanced Raman spectroscopy of nonresonant molecules, J. Am. Chem. Soc. 131, 14466–14472.

[2] Yang, Y., Yang, J., Liang, C., and Wang, H. (2008). Ultra-broadband enhanced absorption of metal surfaces structured by femtosecond laser pulses, Opt. Express 16, 11259–11265.

[3] Wang, F., Chen, C., He, H., and Liu, S. (2011). Analysis of sunlight loss for femtosecond laser microstructured silicon and its solar cell efficiency, Appl. Phys. A 103, 977–982.

[4] Pfuch, A., Güell, F., Toelke et al. (2013). Photocatalytic activities of TiO_2 nanotubes, Proc. SPIE 8626, 8626S1–8626S6.

[5] Kolasinski, K., W. (2012). Surface science: Foundations of catalysis and nanoscience, 3rd Edition, Chichester, John Wiley & Sons.

[6] Bonse, J., Koter, R., Hartelt, M. et al. (2014). Femtosecond laser-induced periodic surface structures on steel and titanium alloy for tribological applications, Appl. Phys. A 117, 103–110.

[7] Liang, C., Wang, H., Yang, J., Li, B., Yang, Y., and Li, H. (2012). Biocompatibility of the micro-patterned NiTi surface produced by femtosecond laser, Appl. Surf. Sci. 261, 337–342.

[8] Susana Pérez, S., Rebollar, E., Oujja, M., Martín, M., and Castillejo, M. (2013). Laser-induced periodic surface structuring of biopolymers, Appl. Phys. A 110, 683–690.

[9] Liang, C., Wang., H., Yang, J. et al. (2013). Femtosecond laser-induced micropattern and Ca/P deposition on Ti implant surface and its acceleration on early osseointegration, ACS Appl. Mater. Interfaces 5, 8179−8186.

[10] Vorobyev, A. Y. and Guo, C. (2009). Femtosecond laser surface structuring of biocompatible metals, Proc. SPIE 7203, 72030O-1.

[11] Lin, C. Y., Chenga, C. W., and Oub, K. L. (2012). Micro/nano-structuring of medical stainless steel using femtosecond laser pulses. Physics Procedia 39, 661–668.

[12] Barberoglou, M., Zorba, V., Stratakis et al. (2009). Bio-inspired water repellent surfaces produced by ultrafast laser structuring of silicon, Appl. Surf. Sci. 255, 5425–5429.

[13] Rukosuyev, M. V., Lee, J., Seong J. C., Lim, G. J., Martin, B. G. (2014). One-step fabrication of superhydrophobic hierarchical strutures by femtosecond laser ablation, Appl. Surf. Sci. 313, 411–417.

[14] Song, S., Jing, L., Fu, S. H., and Luan, Y. (2008). Superhydrophilic anatase TiO_2 film with the micro-and nanometer-scale hierarchical surface structure, Mat. Lett. 62, 3503–3505.

[15] Intravaia, F., Koev, S., Jung, W. et al. (2013). Strong Casimir force reduction through metallic surface nanostructuring, Nature Commun. 4, 2515.

[16] Das, S. K., Messaoudi, H., Debroy, A., McGlynn, E., and Grunwald, R. (2013). Multiphoton excitation of surface plasmon-polaritons and scaling of nanoripple formation in large bandgap materials, Opt. Mat. Express 3, 1705–1715.

[17] Shen, W. C., Cheng, C. W., Yang, M. C., Kozawa, Y., and Sato, S. (2010). Fabrication of novel structures on silicon with femtosecond laser pulses, J. Laser Micro/Nanoeng. 5, 229–232.

[18] Hnatovsky, C., Shvedov, V. G., Krolikowski, W., and Rode, A V. (2010). Materials processing with a tightly focused femtosecond laser vortex pulse, Opt. Lett. 35, 3417–3419.

[19] Drude, P. (1900). Zur Elektronentheorie der Metalle, Ann. Phys. 306, 566–613.

[20] Van Driel, H. M. Sipe, J. E., and Young, J. F. (1982). Laser-induced periodic surface structure on solids: a universal phenomenon, Phys. Rev. Lett. 49, 1955–1958.

[21] Birnbaum, M. (1965). Semiconductor surface damage produced by ruby lasers, J. Appl. Phys. 36, 3688–3689.

[22] Bonse, J., Krüger, J., Höhm, S., and Rosenfeld, A. (2012). Femtosecond laser-induced periodic surface structures, J. Laser Appl. 24, 042006.

[23] Vorobyev, A. Y. and Guo, C. (2013). Direct femtosecond laser surface nano/microstructuring and its applications, Laser Photonics Rev. 7, 285–407.

[24] Spielmann, C. (2015). Laser-plasma-based secondary sources: accelerating particles and light, Frontiers in Optics/Laser Science, FM2A.1.

[25] Elsied, A. M., Termini, N. C., Diwakar, P. K., and Hassanein, A. (2016). Characteristics of Ions Emission from Ultrashort Laser Produced Plasma, Sci. Rep. 6, 38256.
[26] Simanovskii, D. M., Gladskikh, A. N., Shmaenokm, L. A., Bobashev, S. V. (1996). Demonstration of laser induced x-ray generation in an expanding laser produced plasma, Phys Rev Lett. 77, 849-852.
[27] Flory, F., Escoubas, L., and Berginc, G. (2011). Optical properties of nanostructured materials: a review, J. Nanophoton. 5, 052502.
[28] Brissonneau, V., Escoubas, L., Flory, F. et al. (2011). Laser-assisted fabrication of random rough surfaces for optoelectronics, Appl. Surf. Sci. 258, 9171–9174.
[29] Vorobyev, A. Y. and Guo, C. (2005). Enhanced absorptance of gold following multipulse femtosecond laser ablation, Phys. Rev. B 72, 195422.
[30] Csizmadia, T., Smausz, T. Tapai, C. et al. (2015). Comparison of the production of nanostructures on bulk metal samples by picosecond laser ablation at two wavelengths for the fabrication of low-reflective surfaces, J. Laser Micro/Nanoeng. 10, 110–118.
[31] Ahsan, M. S., Ahmed, F., Kim, Y. G. et al. (2011). Colorizing stainless steel surface by femtosecond laser induced micro/nano-structures, Appl. Surf. Sci. 257, 7771–7777.
[32] Vorobyev, A. Y. and Guo, C. (2018). Colorizing metals with femtosecond laser pulses, Appl. Phys. Lett. 92, 041914.
[33] Skjølstrup, E. J. H. and T. Søndergaard, T. (2017). Optics of multiple ultrasharp grooves in metal, J. Opt. Soc. Am. B 34, 673-680.
[34] Vorobyev, A. Y., and Guo, C. (2017). Multifunctional surfaces produced by femtosecond laser pulses, J. Appl., Phys. 117, 033103.
[35] Volkov, S. N., Kaplan, A. E., and Miyazaki (2009). K., Evanescent field at nanocorrugated dielectric surface, APL 94, 0041104.
[36] Ionin, A. A., Kudryashov, S. I., Ligachev, A. E. et al. (2013). Local field enhancement on metallic periodic surface structures produced by femtosecond laser pulses, Quantum Electronics 43, 304–307.
[37] Hou, S., Huo, Y., Xiong, P. (2011). Formation of long- and short-periodic nanoripples on stainless steel irradiated by femtosecond laser pulses, J. Phys. D: Appl. Phys. 44, 505401.
[38] Chen, J. T., Lai, W. C., Kao, Y. J. et al. (2012). Laser-induced periodic structures for light extraction efficiency enhancement of GaN-based light emitting diodes, Opt. Express 20, 5689–5695.
[39] Fleischmann, M., Hendra, P. J., and McQuillan, A. J. (1974). Raman spectra of pyridine adsorbed at a silver electrode, Chem. Phys. Lett. 26, 163–166.
[40] McQuillan, A. J. (2009). The discovery of surface-enhanced Raman scattering, Notres Rec. R. Soc. 63, 105–109.
[41] Blackie, E. J., Le Ru, E. C., Meyer, M., Etchegoin, P. G. (2007). Surface enhanced Raman scattering enhancement factors: A comprehensive study, J. Phys. Chem. C 111, 13794–13803.
[42] Kneipp, K. (2007). Surface-enhanced Raman scattering (feature article), Physics today 60, 40–46.
[43] Kneipp, K., Wang, Y., Kneipp et al. (1997). Single molecule detection using surface-enhanced Raman scattering (SERS), Phys. Rev. Lett. 78, 1667–1670.
[44] Nie, S., Emory, S. R. (1997). Probing single molecules and single nanoparticles by surface-enhanced Raman scattering, Science. 275, 1102–6.
[45] Le Ru, E. C.; Meyer, M., and Etchegoin, P. G. (2006). Proof of single-molecule sensitivity in surface enhanced Raman scattering (SERS) by means of a two-analyte technique, J. Phys. Chem. B. 110, 1944–1948.
[46] Radziuk, D. and Moehwald, H. (2014). Highly effective hot spots for SERS signatures of live fibroblasts, Nanoscale 6, 6115–6126.
[47] Sheremet, E., Milekhin, A. G., Rodriguez, R. D. et al. (2014). Surface- and tip-enhanced resonant Raman scattering from CdSe nanocrystals, Nanoscale 6, 6115–6126.

[48] Li, Z. and Xu, H. (2016). Nanoantenna effect of surface-enhanced Raman scattering: managing light with plasmons at the nanometer scale, Advances in Physics: X 1, 492–521.
[49] Chen, K., Dao, T. D., and Nagao, T. (2017). Tunable nanoantennas for surface enhanced infrared absorption spectroscopy by colloidal lithography and post-fabrication etching, Sci. Rep. 7, 44069.
[50] S.Z. Oo, S. Z., Chen, R. Y., Siitonen, S. et al. (2013). Disposable plasmonic plastic SERS sensor, Opt. Express 21, 18484–18491.
[51] Pfuch, A., Güell, F., Toelke, T. et al. (2013). Photochemical activity of TiO_2 nanotubes, Proc. SPIE 8626, 86260S-1–86260S-6.
[52] Qu, X., Alvarez, P. J. J., and Li, Q. (2013). Applications of nanotechnology in water and wastewater treatment, Water Research 47, 3931–3946.
[53] Khan, S. U. M., Al-Shahry, M., and Ingler Jr., W. B. (2002). Efficient photochemical water splitting by a chemically modified n-TiO_2, Science 297, 2243–2245.
[54] Varghese, O. K., Paulose, M., LaTempa, T. J., and Craig A. Grimes (2009). High-rate solar photocatalytic conversion of CO_2 and water vapor to hydrocarbon fuels, Nanolett. 9, 731–737.
[55] Sohn,Y., Huang, W., and Fariborz, T. (2017). Recent progress and perspectives in the photocatalytic CO2 reduction of Ti-oxide-based nanomaterials, Appl. Surf. Sci. 396, 1696–1711.
[56] Das, S. K., Biswas, M., Byrne et al. (2010). Multiphoton-absorption induced UV luminescence of ZnO nanorods using low-energy fs-pulses, J. Appl. Phys. 108, 043107.
[57] Ogata, Y. (2016). Optical second harmonic generation from nanostructure-covered micro-cubes on nickel, Opt. Mat. Express 6, 1520–1529.
[58] Zhang, X. Q., Tang, Z. K., Kawasaki, M., Ohtomo, A., and Koinuma, H. (2003). Resonant exciton second-harmonic generation in self-assembled ZnO microcrystallite thin films, J. Phys.: Cond. Matter 15, 5191–5196 (2003).
[59] Chan, S. W., Barille, R., Nunzi et al. (2006). Second harmonic generation in zinc oxide nanorods, Appl. Phys. B 84, 351–355.
[60] Das, S. K., Guell, F., Gray, C. et al. (2014). ZnO nanorods for efficient third harmonic UV generation, Opt. Mat. Express 4, 701–709.
[61] Singhal, H., Ganeev, R. A., Naik, P. A. et al. (2010). Study of high-order harmonic generation from nanoparticles, J. Phys. B: At. Mol. Opt. Phys. 43, 025603.
[62] Zhang, C. F., Dong, Z. W., You, G. J., Qian, S. X. (2006). and H. Deng, Multiphoton route to ZnO nanowire lasers, Opt. Lett. 31, 3345–3347.
[63] Bonse, J., Höhm, S., Kirner, S. V., Rosenfeld, A., and Krüger, J. (2017). Laser-induced periodic surface structures - a scientific evergreen, IEEE J. Sel. Top. Quant. Electron. 23, 9000615.
[64] Sipe, J. E., Young, J. F., Preston, J. S., and van Driel, H. M. (1983). Laser-induced periodic surface structure. I. Theory, Phys. Rev. B 27, 1141–1154.
[65] Young, J. F., Preston, J. S., van Driel, H. M., and Sipe, J. E. (1983). Laser-induced periodic surface structure. II. Experiments on Ge, Si, Al, and brass, Phys. Rev. B 27, 1155–1172.
[66] Young, J. F., Sipe, J. E., and van Driel, H. M. (1984). Laser-induced periodic surface structure. III. Fluence regimes, the role of feedback, and details of the induced topography in germanium, Phys. Rev. B 30, 2001–2015.
[67] Brueck, S. R. and Ehrlich, D. J. (1982). Simulated surface-plasma-wave scattering and growth of a periodic structure in laser-photodeposited metal films, Phys. Rev. Lett. 48, 1678–1681.
[68] Kaplan, A. E. and Miyazaki, K. (2007). Laser-induced surface nano-ripples as manifestation of Wigner excitons, Quantum Electronics and Laser Science Conference, QELS '07, QTuE7.
[69] Tsibidis, G. D., Fotakis, C., and Stratakis, E. (2015). From ripples to spikes: A hydrodynamical mechanism to interpret femtosecond laser-induced self-assembled structures. Phys. Rev. B 92, 041405(R).
[70] Costache, F., Eckert, S., and Reif, J. (2006). On ultra-short laser pulse induced instabilities at the surface of non-metallic solids, Proc. SPIE 6261, 626107.

[71] Olga Varlamova (2013). Self-organized surface patterns originating from femtosecond laser-induced instability, Doctoral Thesis, Technical University Cottbus, publisher: Göttingen: Cuvillier, 2014.
[72] Csete, M., Hild, S., Plettl, A., Ziemann, P., Bor, Zs., and Marti, O. (2004). The role of original surface roughness in laser-induced periodic surface structure formation process on poly-carbonate films, Thin Sol. Films 453-454, 114–120.
[73] Obara, G., Maeda, N., Miyanishi, T. et al. (2011). Plasmonic and Mie scattering control of far-field interference for regular ripple formation on various material substrates, Opt. Express 19, 19093–19103.
[74] Kudryashov, S. I., Makarov, S. V., Ionin, A. A. et al. (2015). Dynamic polarization flip in nanoripples on photoexcited Ti surface near its surface plasmon resonance. Opt Lett. 40, 4967–70.
[75] Bonse, J., Rosenfeld, A., and Krüger, J. (2012). Femtosecond laser-induced periodic surface structures: recent approaches to explain their sub-wavelength periodicities, Proc. SPIE 7994, 79940M-7.
[76] van Driel, H. M. and Dworschak, K. (1992). Locking of optical and thermodynamic length scales in laser-induced melt-solid patterns on silicon, Phys. Rev. Lett. 69, 3487–3490.
[77] Jia, T. Q., Chen, H. X., Huang et al. (2005). Formation of nanogratings on the surface of a ZnSe crystal irradiated by femtosecond laser pulses, Phy. Rev. B 72, 125429.
[78] Wagner, R., Gottmann, J., Horn, A., and Kreutz, E. W. (2006). Subwavelength ripple formation induced by tightly focused femtosecond laser radiation, Appl. Surf. Sci. 252, 8576–8579.
[79] Zhao, Q. Z., Malzer, S., and Wang, L. J. (2007). Formation of subwavelength periodic structures on tungsten induced by ultrashort laser pulses, Opt. Lett. 32, 1932–1934.
[80] Ganeev, R. A. (2009). Formation of different periodic nanostructures on semiconductors, Optics and Spectroscopy 106, 142–146.
[81] Le Harzic, R., Schuck, H., Sauer et al. (2005). Sub-100 nm nanostructuring of silicon by ultrashort laser pulses, Opt. Express 13, 6651–6656.
[82] Dufft, D., Rosenfeld, A., Das, S. K., Grunwald, R., and Bonse, J. (2009). Femtosecond laser-induced periodic surface structures revisited: A comparative study on ZnO, J. Appl. Phys. 105, 034908.
[83] Das, S. K., Messaoudi, H., Debroy, A., McGlynn, E., and Grunwald, R., Multiphoton excitation of surface plasmon-polaritons and scaling of nanoripple formation in large bandgap materials, Opt. Mat. Express 3, 1705–1715 (2013).
[84] Das, S. K., Dufft, D., Rosenfeld et al. (2009). Femtosecond-laser-induced quasiperiodic nanostructures on TiO_2 surfaces, J. Appl. Phys. 105, 084912.
[85] Huang, M., Cheng, Y., Zhao, F., and Xu, Z. (2013). The significant role of plasmonic effects in femtosecond laser-induced grating fabrication on the nanoscale, Ann. Physik 525, 74–86.
[86] Garrelie, F., Colombier, J. P., Pigeon, F. et al. (2008). Evidence of surface plasmon resonance in ultrafast laser-induced ripples, Opt. Express 19, 9035–9043.
[87] Robitaille, A., Boulais, E., and Meunier, M., (2013). Mechanisms of plasmon-enhanced femtosecond laser nanoablation of silicon, Opt. Express 21, 9703–9710.
[88] Derrien, T. J. -Y., Itina, T. E., Torres, R., Sarnet, T., and Sentis, M. (2013). Possible surface plasmon polariton excitation under femtosecond laser irradiation of silicon, J. Appl. Phys. 114, 083104 (2013).
[89] Derrien, T. J. -Y., Krüger, J., Itina, T. E. et al. (2014). Rippled area formed by surface plasmon polaritons upon femtosecond laser double-pulse irradiation of silicon, Appl. Phys. A 117, 77–81.
[90] Zhu, J.-T., Shen, Y.-F., Li, W. et al. (2006). Effect of polarization on femtosecond laser pulses structuring silicon surface, Appl. Surf. Science 252, 2752–2756.
[91] Ionin A. A., Kudryashov, S. I., Makarov, S. V. et al. (2016). Nanoscale surface boiling in sub-threshold damage and above-threshold spallation of bulk aluminum and gold by single femtosecond laser pulses, Laser Phys. Lett. 13, 025603 (2016).

[92] Rämer, A., Haahr-Lillevang, L., Rethfeld, and B., Balling, P. (2016). Modeling the transient optical parameters in laser-excited band gap materials, Opt. Eng. 56, 011015.
[93] Li, C., Feng, D., Jia, T. et al. (2005). Ultrafast dynamics in ZnO thin films irradiated by femtosecond lasers, Solid State Comm. 136, 389–394 (2005).
[94] Colombier, J.-P., Garrelie, F., Brunet, P. et al. (2012). Advances in understanding how femtosecond laser ripples formation in metal works, LASERAP'7, Oct. 2012, Oléron, France, pp. 294–299, hal-00753853.
[95] Nathala, C. S. R., Ali, A., Ionin, A. A. et al. (2015). Experimental study of fs-laser induced sub-100-nm periodic surface structures on titanium, Opt. Express 23, 5915–5929.
[96] Zimmermann, F., Plech, A., Richter, S., Tünnermann, A., and Nolte, S. (2016). The onset of ultrashort pulse-induced nanogratings, Laser Photon. Rev. 10, 327–334.
[97] Garcia-Lechuga, M., Puerto, D., Fuentes-Edfuf, Y., Solis, J., and Siegel, J. (2016). Ultrafast moving-spot microscopy: birth and growth of laser-induced periodic surface structures, ACS Photonics 3, 1961–1967.
[98] Höhm, S., Rosenfeld, A., Krüger, J., and Bonse, J. (2013). Area dependence of femtosecond laser-induced periodic surface structures for varying band gap materials after double pulse excitation, Appl. Surf. Sci. 278, 7–12.
[99] Rosenfeld, A., Rohloff, M., Höhm, S., Krüger, J., and Bonse, J. (2012). Formation of laser-induced periodic surface structures on fused silica upon multiple parallel polarized double-femtosecond-laser-pulse irradiation sequences, Appl. Surf. Sci. 258, 9233–9236.
[100] Höhm, S., Rosenfeld, A., Krüger, J., and Bonse, J. (2017). Laser-induced periodic surface structures on zinc oxide crystals upon two-colour femtosecond double-pulse irradiation, Phys. Scr. 92, 034003.
[101] Reich, C., Uschmann, I., Ewald, F. et al. (2003). Spatial characteristics of Kα emission from relativistic femtosecond laser pulses, Phys. Rev. E 68, 056407.
[102] Zamponi, F., Lübcke, A., Kämpfer, T. et al. (2010). Directional bremsstrahlung from a Ti laser-produced x-ray source at relativistic intensities in the 3-12 keV range, Phys. Rev. Lett. 105, 085001.
[103] Thaury, C. and Quéré, F. (2010). High-order harmonic and attosecond pulse generation on plasma mirrors: basic mechanism, J. Phys. B: At. Mol. Opt. Phys. 43, 213001.
[104] Gibbon, P. (2005). Short pulse laser interaction with matter. (1st edn.). London: Imperial College Press.
[105] Daido, H., Nishiuchi, M., and Pirozhkov, A. S. (2012). Review of laser-driven ion sources and their applications, Rep. Prog. Phys. 75, 056401.
[106] Macchi, A., Borghesi, M., and M. Passoni (2013). Ion acceleration by superintense laser-plasma interaction, Rev. Mod. Phys. 85, 751–793.
[107] Kim, I. J., Pae, K. H., Choi, I. W. et al. (2016). Radiation pressure acceleration of protons to 93 MeV with circularly polarized petawatt laser pulses, Phys. Plasmas 23, 070701.
[108] Hegelich, B. M., Jung, D., Albright, B. J. et al. (2013). 160 MeV laser-accelerated protons from CH2 nano-targets for proton cancer therapy, arXiv:1310.8650.
[109] Tajima, T., Habs, D., and Yan, X. (2009). Laser acceleration of ions for radiation therapy, Rev. Accel. Sci. Tech. 2, 201-228.
[110] Schardt, D., Elsässer, T., and Schulz-Ertner, D. (2010). Heavy-ion tumor therapy: Physical and radiobiological benefits, Rev. Mod. Phys. 82, 383–425.
[111] Steinke, S., Henig, A., Schnürer, M. et al. (2010). Efficient ion acceleration by collective laser-driven electron dynamics with ultra-thin foil targets, Laser Part. Beams 28, 215–221.
[112] Brenner, C. M., Robinson, A. P. L., Markey, K. et al. (2014). High energy conversion efficiency in laser-proton acceleration by controlling laser-energy deposition onto thin foil targets, Appl. Phys. Lett. 104, 081123.
[113] Takahashi, K., Kawata, S., Satoh, D., Ma, Y. Y., Barada, D., and Kong, Q. (2010). Efficient energy conversion from laser to proton beam in a laser-foil interaction, Phys. Plasmas 17, 093102.

[114] Klimo, O., Psikal, J., Limpouch, J. et al. (2011). Short pulse laser interaction with microstructured targets: simulations of laser absorption and ion acceleration, New J. Phys., 13, 053028.
[115] Andreev, A. A. and Platonov, K. Y. (2011). Kα radiation of foil under interaction with laser pulse of relativistic intensity, Optics and Spectroscopy 110, 20–23.
[117] Andreev, A., Platonov, K., Braenzel, J. et al. (2015). Relativistic laser nano-plasmonics for effective fast particle production, Plasma Phys. Control. Fusion 58, 014038.
[117] Margarone, D., Klimo, O., Kim, I. J. et al. (2012). Laser-driven proton acceleration enhancement by nanostructured foils, Phys. Rev. Lett. 109, 234801.
[118] Margarone, D., Kim, I. J., Psikal, J. et al. (2015). Laser-driven high-energy proton beam with homogeneous spatial profile from a nanosphere target, Phys. Rev. Spec. Topics - Accelerators and Beams 18, 071304.
[119] Floquet, V., Klimo, O., Psikal, J. et al. (2013). Micro-sphere layered targets efficiency in laser driven proton acceleration, J. Appl. Phys. 114, 083305.
[120] Zigler, A., S. Eisenman, Botton, M. et al. (2013). Enhanced proton acceleration by an ultrashort laser interaction with structured dynamic plasma targets, Phys. Rev. Lett. 110, 215004.
[121] Passoni, M., Zani, A., Sgattoni, A. et al. (2014). Energetic ions at moderate laser intensities using foam-based multi-layered targets, Plasma Phys. Control. Fusion 56, 045001.
[122] Prencipe, I., Sgattoni, A., Dellasega, D. et al. (2016). Development of foam-based layered targets for laser-driven ion beam production, Plasma Phys. Control. Fusion 58, 034019.
[123] Ceccotti, T., Floquet, V., Sgattoni, A. et al. (2013). Evidence of resonant surface-wave excitation in the relativistic regime through measurements of proton acceleration from grating targets, Phys. Rev. Lett. 111, 0185001.
[124] Qiao, B., Zepf, M., Borghesi, M. et al. (2010). Radiation-pressure acceleration of ion beams from nanofoil targets: The leaky light-sail regime, Phys. Rev. Lett. 105, 155002.
[125] Bin, J. H., Ma, W. J., Wang, H. Y. et al. (2015). Ion acceleration using relativistic pulse shaping in near-critical-density plasmas, Phys. Rev. Lett. 115, 064801.
[126] Tsukamoto, M., Asuka, K., Nakano, H. et al. (2006). Periodic microstructures produced by femtosecond laser irradiation on titanium plate, Vacuum 80, 1346–1350.
[127] Guo, C. and Vorobyev, A. Y. (2007). Femtosecond laser structuring of titanium implants, Appl. Surf. Sci. 253, 7272–7280.
[128] Huang, Y., Liu, S., Li, W., Liu, Y., and W. Yang (2009). Two-dimensional periodic structure induced by single-beam femtosecond laser pulses irradiating titanium, Opt. Express 17, 20756-20761.
[129] Okamuro, K., Hashida, M., Miyasaka, Y. et al. (2010). Laser fluence dependence of periodic grating structures formed on metal surfaces under femtosecond laser pulse irradiation, Phys. Rev. B 82, 165417.
[130] Bonse, J., Krüger, J., Höhm, S., and Rosenfeld, A. (2012). Femtosecond laser-induced periodic surface structures, J. Laser Appl. 24, 042006.
[131] Bonse, J., Höhm, S., Rosenfeld, A., and Krüger. J. (2013). Sub-100-nm laser-induced periodic surface structures upon irradiation of titanium by ti:sapphire femtosecond laser pulses in air, Appl. Phys. A 110, 547–551.
[132] Lübcke, A., Andreev, A. A., Höhm, S. et al. (2017). Prospects of target nanostructuring for laser proton acceleration, Sci. Rep. 7, 44030.
[133] Kaluza, M., Schreiber, J., Santala, M. I. K. et al. (2004). Influence of the laser prepulse on proton acceleration in thin-foil experiments, Phys. Rev. Lett. 93, 045003.
[134] Neely, D., Foster, P., Robinson, A. et al. (2006). Enhanced proton beams from ultrathin targets driven by high contrast laser pulses, Appl. Phys. Lett. 89, 021502.
[135] Dalui, M., Kundu, M., Madhu, T. et al. (2014). Bacterial cells enhance laser driven ion acceleration, Sci. Rep. 4, 06002.

[136] Quéré, F., Thaury, C., Monot, P. et al. (2006). Coherent Coherent Wake Emission of High-Order Harmonics from Overdense Plasmas, Phys. Rev. Lett. 96, 125004.
[137] Dromey, B., Rykovanov, S., Yeung, M. et al. (2012). Coherent synchrotron emission from electron nanobunches formed in relativistic laser-plasma interactions, Nature Phys. 8, 804–808.
[138] Andreev, A. A. and Platonov, K. Y. (2016). X-ray generation by fast electrons propagating in nanofibres irradiated by a laser pulse of relativistic intensity, Quant. Electron. 46, 109–118.
[139] Braenzel, J., Ehrentraut, L., Platonov, K. Y., Andreev, A., and Schnuerer, M. (2017). Amplification of coherent synchrotron-like high harmonic emission from ultra-thin foils in relativistic light fields, to be published.
[140] Xu, H., Hajisalem, G., Steeves, G. M. et al., (2015). Nanorod surface plasmon enhancement of laser-Induced ultrafast demagnetization, Sci. Rep. 5, 15933.
[141] Maradudin, A. A. (2011). Structured surfaces as optical metamaterials. (1st edn.). Cambridge: Cambridge University Press.
[142] Lévy, A., Ceccotti, T., D'Oliveira, P. et al. (2007). Double plasma mirror for ultrahigh temporal contrast ultraintense laser pulses, Opt. Lett. 32, 310–312.
[143] Hawkeye, M. M. and Brett, M. J. (2007). Glancing angle deposition: fabrication, properties, and applications of micro-and nanostructured thin films, J. Vac. Sci. Technol. 25, 1317–1335.
[144] Veselago, V. G. (1968). The electrodynamics of substances with simultaneously negative values of ϵ and μ, in: Sov. Phys. Usp. 10, 509–514.
[145] McGlynn, E., Henry, M. O., Mosnier, J.-P. (2009). ZnO wide bandgap semiconductor nanostructures: growth, characterisation and applications. In Narlikar, A. V., and Fu, Y. Y., (eds.) Handbook of nanoscience and technology vol. II, Oxford: Oxford University Press.
[146] Güell, F., Osso, J. O., Goni, A. R. et al. (2009). Synthesis and optical spectroscopy of ZnO nanowires, Superlatt. Microstruct. 45, 271–276.
[147] Sakabe, M., Lienau, C., and Grunwald, R. (Eds.) (2015). Progress in Nonlinear Nano-Optics, Heidelberg: Springer-Verlag.
[148] Simmons, J. F. L. and McInnes, C. R. (1993). Was Marx right? or How efficient are laser driven interstellar spacecraft? Am. J. Phys. 61, 205–207.
[149] Gardiner, D. J. (1989). Practical Raman spectroscopy. Berlin: Springer-Verlag.
[150] Wang, S. and Jiang, L. (2007). Definition of superhydrophobic states. Adv. Mat. 19, 3423–3424.
[151] Kalashnikov, M., Osvay, K., Volkov, R., Schönnagel, H., and Sandner, W. (2011). High temporal contrast front end with a multipass Ti:sa amplifier and a CaF_2-based XPW temporal filter. In CLEO:2011 - Laser Applications to Photonic Applications, CWG3. Washington: Optical Society of America.
[152] Minkovski, N., Petrov, G. I., Saltiel, S. M., Albert, O., and Etchepare, J. (2004). Nonlinear polarization rotation and orthogonal polarization generation experienced in a single-beam configuration, J. Opt. Soc. Am. B 21, 1659–1664.

Further Reading

Brabec, Th. (ed.) (2008). Strong-field Laser Physics. (1st edn.). New York: Springer.
Cao, G. (2004). Nanostructures and nanomaterials: Synthesis, properties and applications, London, Imperial College Press.
Di Fabrizio, E., Schlücker, S., Wenger, J. et al. (2016). Roadmap on biosensing and photonics with advanced nano-optical methods, J. Opt. 18, 063003.
Djurisic, A. B. and Leung, Y. H. (2006). Optical properties of ZnO nanostructures, small 2, 944–961.
Haghi, A. K., Zachariah, A. K., and Kalariakkal, N. (2012). Nanomaterials: synthesis, characterization, and applications. (1st edn.). Oakville: Apple Academic Press.
Hommelhoff, P., Kling, M., Stockman, M. (eds.) (2013). Special Issue: Ultrafast phenomena on the nanoscale, Ann. Physik, 525, A1–A24, 1–204, L1–L22.

Pitarke, J. M., Silkin, V. M., Chulkov, E. V., and Echenique, P. M. (2007). Theory of surface plasmons and surface-plasmon polaritons, Rep. Prog. Phys. 70, 1–87.
Sarid, D. and Challener, W. A. (2010). Modern introduction to surface plasmons: Theory, mathematica modeling, and applications. (1st edn.). Cambridge University Press.
Scott, S. L., Crudden, C. M., and Jones, C. W. (2003), (1st edn.). Nanostructured Catalysts, New York: Kluwer Academic Publishers (since 2005: Springer Science & Business Media).
Shahbazyan, T. V. and Stockman, M. I. (2013). Plasmonics: Theory and applications. (1st edn.). Berlin: Springer-Verlag.
Sivakumar, P. M., Kodolov, V. I., Zaikov, G. E. and Haghi, A. K. (2014). Nanostructure, nanosystems, and nanostructured materials: theory, production and development. (1st edn.). Oakville: Apple Academic Press.
Stockman, M. (2011). Nanoplasmonics: The physics behind the applications (feature article), Physics today 64, 39–44.
Yamashita, H. and Li, H. (2016). Nanostructured photocatalysts: Advanced functional materials (nanostructure science and technology). (1st edn.). Cham: Springer International Publishing.
Zhuiykov, S. (2013). Nanostructured semiconductor oxides for the next generation of electronics and functional devices. (1st edn.). Woodhead Publishing (Elsevier).

Figures and figure captions

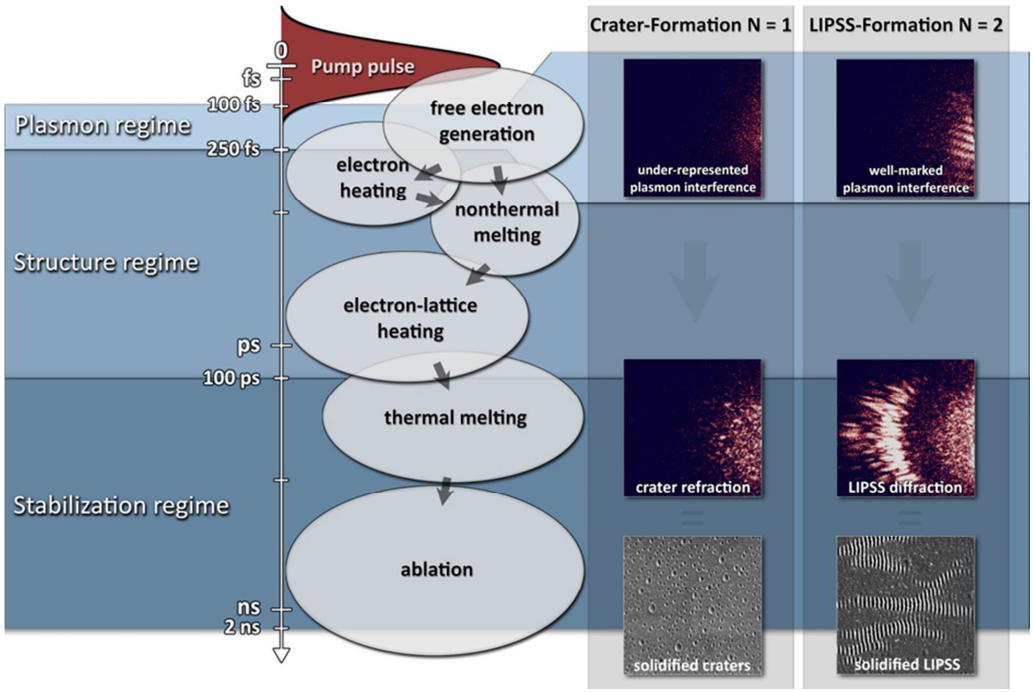

Figure 1 Temporal dynamics of LIPSS formation in silicon. Right side: pump-probe diffraction experiment, left side: corresponding regime and assumed steps of the mechanism (schematically). A combined mechanism is indicated. Plasmons appear during the laser pulse. The nonthermal phase is followed by thermal processes and material re-arrangement.

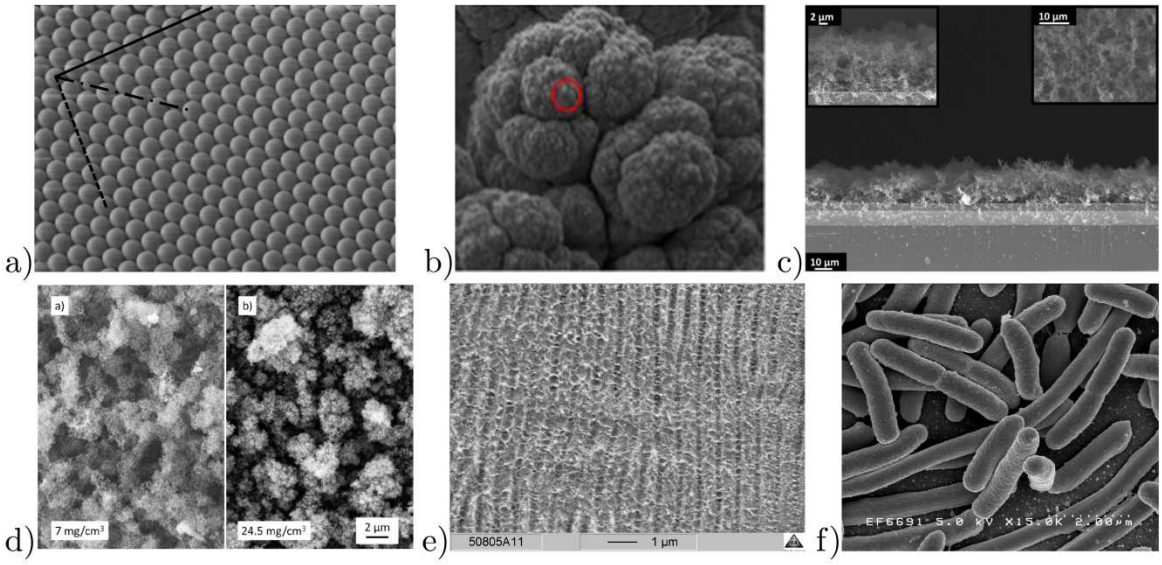

Figure 2 Different nanostructured surfaces used in laser ion acceleration. a) Microsphere targets (with kind permission of J. Appl. Phys. [119]), b) snow target (from [120]), c) foam target (from [121]), d) foam target (from [122]), e) LIPSS (own work), f) E-coli bacteria (Credit: Rocky Mountain Laboratories, NIAID, NIH - NIAID).

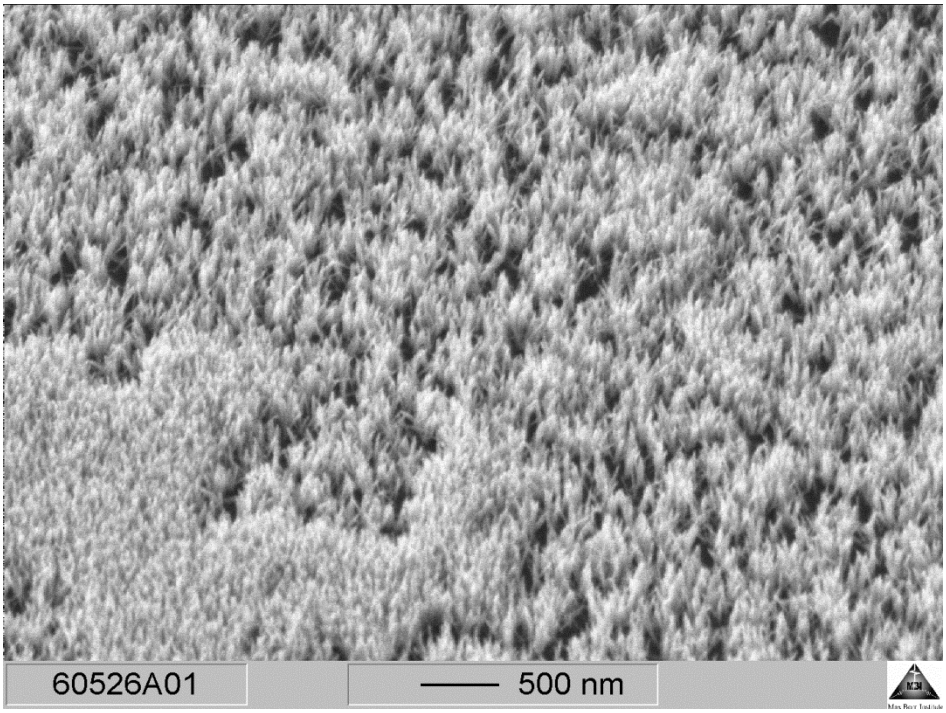

Figure 3 SEM image of a ZnO nanorod sample grown on a 30 nm thick Si_3N_4 substrate.

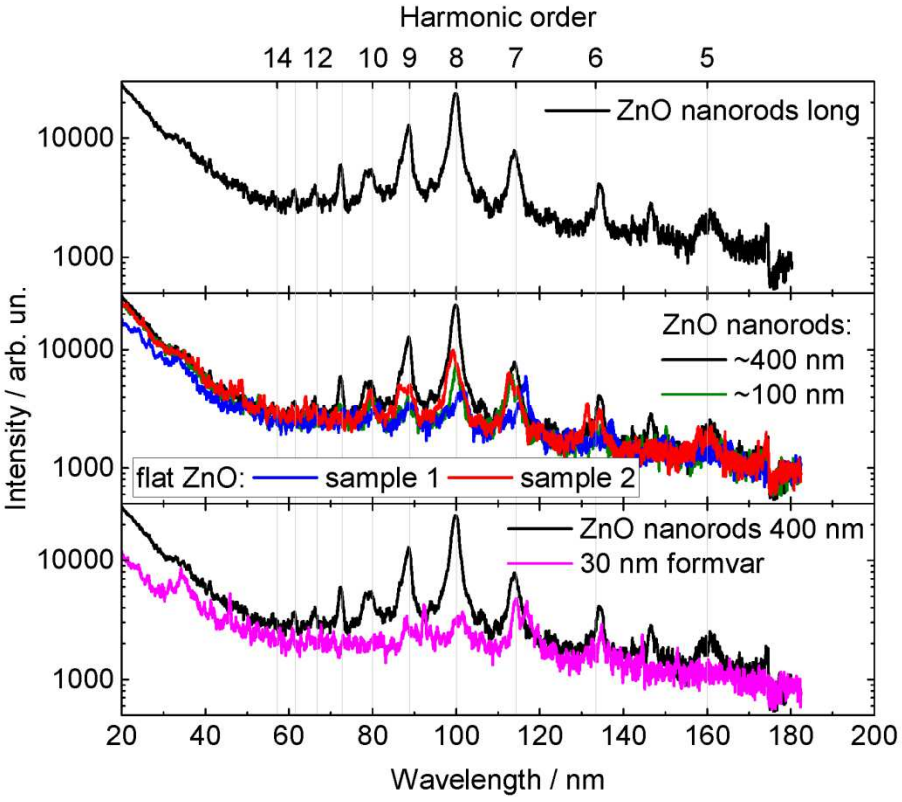

Figure 4 XUV emission spectra for different targets (logarithmic plot). The most efficient long ZnO nanorods (black curve) are compared to short ZnO nanorods (green), flat ZnO layers (red and blue) and formvar (polyvinyl formal resin, pink). All ZnO layers were prepared on a 30 nm thick Si_3N_4 substrate.